DOI 10.5162/sensoren2024/P07

Design of a highly accurate low-cost thermistor-based sensor for the measurement of water surface temperatures in maritime research

Finn Jannek Klar[1], Niklas Torz[1], Thorsten Alexander Kern[1]
[1]Institute of Mechatronics in Mechanics (iMEK), Hamburg University of Technology, Eißendorfer Straße 38, 21073 Hamburg, Germany

Summary

In climate and oceanographic research, precise temperature measurements within the very limited temperature range of the ocean are essential. This paper covers the design and analysis of a temperature sensor that measures with millikelvin accuracy. The first prototype has an energy consumption of 84.64 mWs with a sampling time of 10 seconds per measurement and a component cost of less than 100 EUR. The proposed design is able to measure within 6 mK accuracy on a subset measurement range despite a simple three-point calibration. The core circuit is enhanced with two temperature sensing elements to allow for an increase in sensor sensitivity. A further approach on sensor readout is proposed and analyzed, showing good potential in combination with linearized temperature compensation for the major part of this sensors range.

Keywords: temperature sensor, oceanography, thermistor, water surface

1. Introduction

In ocean and climate research, temperature sensors are subject to high demands. Common models used in ocean research provide measurements in the range from -5 °C to 40 °C with an accuracy of 5 mK and below. These sensors are designed for use at depths of several kilometers and are costly due to the required measurement uncertainty. Especially research projects suffer that require a large number of simultaneously active measuring points. This is particularly relevant for the investigation of submesoscale processes of vertical heat transport in the ocean [1], which are only partially or not at all covered by satellite-based observations with finite resolution and limited observation time.

Our approach focuses on the development of a low-cost temperature sensor capable of measuring water surface temperatures from the surface to a few meters below the waterline at a frequency of 6 min^{-1}. The sensor uses a modified version of an already known analog-to-digital converter circuit (ADC) [2] based on an integrator and an alternating Wheatstone bridge.

In the subsequent sections, we outline the principles of thermistor-based temperature measurement, derive our design based on the work of Skinner and Lambert [2], analyze the circuit and its influences, and present a test showcasing the performance of our temperature measurement approach.

2. Sensor design

A significant portion of temperature sensors utilized in oceanography relies on Wien bridge oscillators (WB) integrated with a thermistor. This integration facilitates a temperature-responsive frequency change in a resonant circuit [3]. Another method, introduced by Skinner and Lambert [2], employs a voltage-to-frequency converter utilizing a switched Wheatstone bridge (WhB) equipped with a thermistor. Makinwa's overview of temperature sensors [4] indicates that both approaches are well-suited for our measurement requirements, offering resolution capabilities down to the microkelvin range. Due to a less complex design, our approach uses a modified version of Skinner and Lambert's circuit.

2.1 Sensing the temperature

The sensitive element of the measuring circuit uses a measuring resistor with a distinct temperature-resistance characteristic. For the realization of this element, negative temperature coefficient (NTC) thermistors are more suitable than metal resistance thermometers in the desired temperature range, as they offer higher sensitivity and a wider resistance range at a lower price.

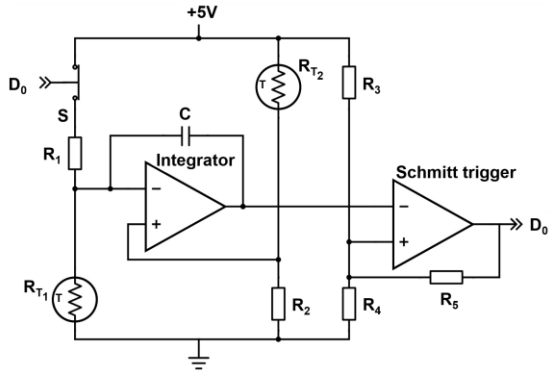

Fig. 1: Structure of the analog-to-digital converter circuit. A Wheatstone bridge circuit is allocated on the left, containing the thermistors R_T1 and R_T2 in opposing legs and the integrator in its center. On the right is the Schmitt trigger, whose switching thresholds are set via resistors R3, R4, and R5, converting the integrator's analog signal into a digital output D0, which is fed into the switch at the top left.

We use the NXFT15WF104FEAB045 from Murata Electronics, which has a resistance of 472 kΩ at -5 °C and 51 kΩ at 40 °C.
The relationship between the temperature T of the thermistor and its resistance R is approximated with sufficient accuracy by the Steinhart-Hart equation [5], a third-order logarithmic polynomial with the component-specific coefficients A, B, and C.

$$T^{-1} = A + B\log R + C(\log R)^3 \tag{1}$$

2.2 Circuit structure and mode of operation

The structure of the ADC circuit is similar to that of Skinner and Lambert but differs from it in key points. Our core circuit (Fig. 1) uses two operational amplifiers (MIC920YC5) and an analog switch (TS5A3167), accessed by the second operational amplifier output line to convert the temperature information into a pulsed signal of varying pulse duration and frequency. A microcontroller decodes this information, to form a 16-bit ADC. In contrast to the design by Skinner and Lambert, the microcontroller is only performing logic functions.
The core circuit translates the temperature information picked up by the thermistor resistance via two stages into binary information. The first stage consists of an alternated Wheatstone bridge, feeding an integrator to create a time-dependent signal.

The upper left leg of the bridge combines a switch S and a resistor R_1 for resetting the integrator, while the lower left leg provides the current through the temperature-sensing thermistor R_{T1} for integration. The two right legs combine a second thermistor R_{T2} and an additional resistor R_2 into a voltage divider. Its reference voltage is fed into the noninverting input of the integrator, defining the voltage across the thermistor R_{T1}.
The second stage uses a Schmitt trigger to convert the time-dependent signal from the integrator output into binary one-bit information. The resistors R_3, R_4, and R_5 are of the same value, setting the trigger levels for high output to 1/3 and the low output trigger level to 2/3 of the supply voltage. This is done to keep the integrator's amplifier within the linear output region close to the supply voltage levels of GND and 5 V.
The digital output signal triggers the switch of the first stages of the Wheatstone bridge, switching between charging and resetting the integrator. Relocating the task of alternating the bridge's operation mode from a microcontroller [2] toward the already existing hardware logic has two effects. It reduces computational effort for circuit control, dropping a previously required interrupt routine and ensuring a synchronous switching of the Wheatstone bridge as soon as the analog signals meet switching criteria. The previous circuit allowed for deviation in monitored and actual charging times caused by a delay between raising an interrupt flag and the interrupt execution. Adding a second thermistor into the sensing circuit of Skinner and Lambert adds a temperature dependency to the voltage across the charging thermistor R_{T1}, increasing the sensitivity by a factor of 2 (Fig. 2).

2.3 Design of the bridge circuit

The right bridge leg uses a voltage divider containing the resistor R_2 and thermistor R_{T2} to feed a temperature-dependent portion of the supply voltage V_+ into the noninverting input of the integrator, which is U_{OP+}:

$$U_{OP+} = V_+ \cdot \frac{R_2}{R_{T_2} + R_2} \tag{2}$$

The voltage on the inverting input U_{OP-} created by the current I_{RT1} through the thermistor R_{T1} is:

$$U_{OP-} = I_{R_{T1}} \cdot R_{T_1}. \tag{3}$$

Due to the restrictions for an ideal operational amplifier, the equation for the voltage on the capacitor during charging is

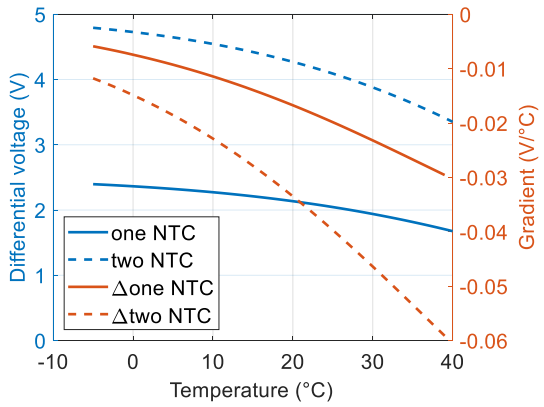

Fig. 2: Comparison of the output voltages of the measuring bridges with one and two NTC thermistors (blue). The gradients (red) display the sensitivity toward temperature-induced changes of the bridges opposing thermistors.

$$\frac{dU_{C,chg}}{dt}\cdot C = V_+ \cdot \frac{R_2}{R_{T_1}(R_{T_2}+R_2)} \tag{4}$$

which leads to

$$U_{C,chg} = \frac{1}{C}\cdot V_+ \cdot \frac{R_2}{R_{T_1}(R_{T_2}+R_2)}\cdot t + U_0 \quad . \tag{5}$$

U_0 is the initial voltage of the capacity when charging. Taking into account that the voltage during charging starts at 1/3 V_+ and ends at 2/3 V_+ the time for charging is

$$t_{chg} = \frac{1}{3}\cdot C \cdot \frac{R_{T_1}(R_{T_2}+R_2)}{R_2} \quad . \tag{6}$$

With U_C reaching 2/3 V_+ the Schmitt trigger closes the switch, resulting in a discharging of the capacity C as R_1 is now connecting V_+ to C. The voltages on the inputs of the integrating operational amplifier remain as in Eq. (2) and Eq. (3). The current through R_1 is

$$I_{R_1} = \frac{V_+ - U_{OP-}}{R_1} \tag{7}$$

Exchanging U_{OP-} with U_{OP+} and applying (3) leads to

$$I_{R_1} = V_+ \cdot \frac{R_{T_2}}{R_1(R_{T_2}+R_2)} \tag{8}$$

Since the current on the capacity, I_C splits now into I_{RT1} and I_{R1}, the equation for the voltage during discharging applied on the capacitor is

$$\frac{dU_{C,dchg}}{dt}\cdot C = V_+ \cdot (A - B) \tag{9}$$

Using

$$A = \frac{R_{T_2}}{R_1(R_{T_2}+R_2)} \tag{10}$$

and

$$B = \frac{R_2}{R_{T_1}(R_{T_2}+R_2)} \tag{11}$$

for abbreviating the equations. From Eq. (9) the time for discharging the capacitor from 2/3 V_+ to 1/3 V_+ is derived equivalent to Eq. (4) to Eq. (6):

$$t_{dchg} = \frac{1}{3}\cdot C \cdot \frac{1}{(A-B)} \tag{12}$$

The duration t_{cycle} of a charging and discharging cycle is the sum of (6) and (12). Assuming that R_{T1} and R_{T2} use identical thermistors this duration is:

$$t_{cycle} = \frac{1}{3}\cdot C \cdot \frac{R_T^4 + R_2 R_T^3}{R_2(R_T^2 - R_1 R_2)} \tag{13}$$

The amount n_{cycles} describes the number of cycles counted during an observation window of length t_{window}:

$$n_{cycles} = \frac{t_{window}}{t_{cycle}} \tag{14}$$

This circuit stops working for higher temperatures when $R_T^2 < R_1 R_2$. To ensure a resolution of 1 mK in the limited range of -5 °C to +40 °C, a minimum difference of two counting cycles per temperature step is required. The calibration temperature of the Wheatstone bridge determines the limit up to which the number of counting cycles can be clearly traced back to temperature values. In the prototype, t_{window} is set to one second, so that the capacitance C must be 10 pF (Fig. 3). Fig. 4 shows a calibration for >50°C as desired and shows that the number of n_{cycles} at the calibration temperature is zero. The calibration temperature is set to 60°C since the minimum number of n_{cycles} per temperature step required to distinguish between two adjacent temperature values cannot be achieved at 50°C (Fig. 5).

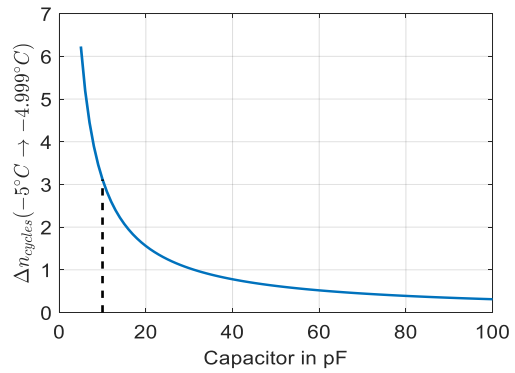

Fig. 3: Influence of the capacitor on the difference in n_{cycles} on the lower temperature range R_1 and R_2 (Eq. (13)) are 22 kΩ, t_{window} is 1 s.

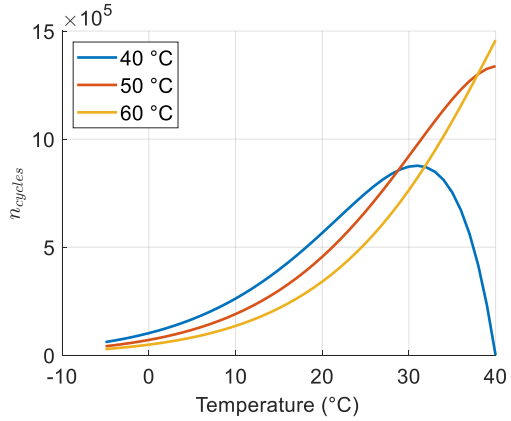

Fig. 4: Influence of different calibration temperatures on the number of counted cycles n_{cycles}.

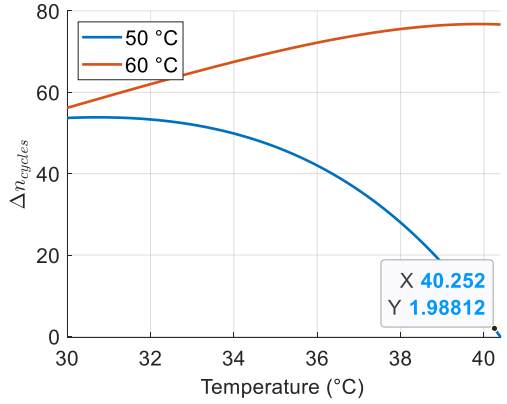

Fig. 5: Step size of the number of n_{cycles} to the next measured value at increased temperature. The temperature increment of this graph is 0.001 °C to display the gradient.

Tab. 1: Parameters for fitting the NTC thermistors resistivity curve to temperatures from -10 °C to 80 °C

Parameter	Value
a_0	3.57e +05
a_1	−1.958e +04
a_2	598
a_3	-13.46
a_4	0.2514
a_5	-0.004054
a_6	5.336e -05
a_7	-5.052e -07
a_8	2.902e -09
a_9	-7.402e -12

The required resistance is about 22 kΩ. A 9th-degree polynomial fitted to the manufacturer's specifications for -10 °C to 80 °C using the MATLAB curve-fitting toolbox gives the thermistor resistance data used for the plot in Fig. 3 and Fig. 5. The polynomial has the form

$$f(x) = \sum_{n=0}^{9} a_n x^n \ . \qquad (15)$$

using the parameters from Tab. 1.

3. Influence Analysis on the Measuring Circuit

Measuring circuits are susceptible to various sources of error, making it essential to consistently consider their behavior under different conditions to ensure accurate sensor output. Among the most common deviations are those resulting from temperature changes in electrical components and variations in production tolerances. Understanding these factors is crucial for mitigating inaccuracies in sensor measurements.

3.1 Influence of temperature on the measuring circuit

The properties of electrical components change with their temperature. Tab. 2 shows these drift coefficients for the components of the integrator bridge circuit. The reference temperature is 25 °C. Based on Eq. 14, temperature drift has a major impact on the ability to provide accurate sensor measurements (Fig. 6). Using the inverse of this curve compensates for the temperature effect on the sensor measurement. Extracting the segments outside the threshold range indicates two areas of linear temperature error compensation (Fig. 7).

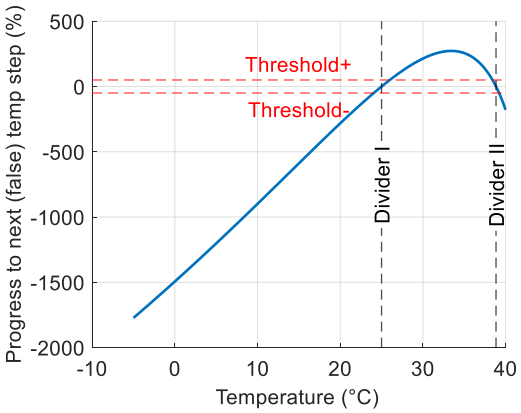

Fig. 6: Temperature-related deviation of the reading compared to the next temperature step of the idealized system. The n_{cycles} values of the idealized system and the temperature-influenced system were subtracted. The result was divided by the step size from the temperature points to the next temperature point, as the number of n_{cycles} separating the temperature readings is different (Fig. 5). The threshold +/- area indicates an area where the deviation between ideal and real value is below 50 % of the step size towards the next temperature value (ideal system)

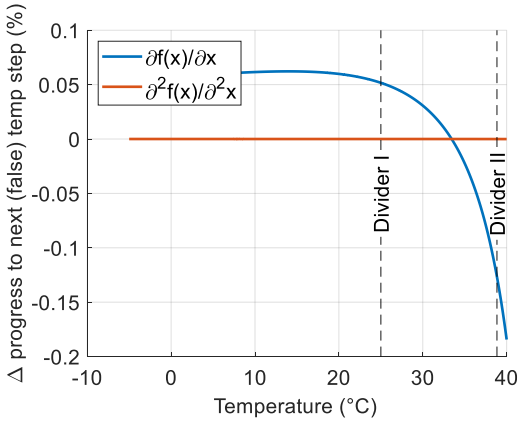

Fig. 7: Numerical derivation of the temperature induced deviation (Fig. 6). The zero crossings of the deviation lead to a segmentation of its derivation. The first segment shows the most linear behavior of the derivative.

Tab. 2: Temperature drift coefficient of components in use.

Component	Temperature drift	Part
C	30 ppm/°C	GRM1555C1H102FA01D
R_1, R_2	100 ppm/°C	AC0805FR-0722KL

3.2 Influence of production tolerance on the measuring circuit

The temperature deviations (Tab. 2) have an insignificant influence on the measured value compared to the manufacturing tolerances (Tab. 3), as the deviation at component level is orders of magnitude greater. The effects of these deviations require comprehensive calibration of the finished sensor (Fig. 8).

Tab. 3: Manufacturing tolerances

Component	Tolerance	Part
C	± 5 %	GRM1555C1H102FA01D
R_1, R_2	± 1 %	AC0805FR-0722KL
R_{T1},R_{T2}	± 1 %	NXFT15WF104FEAB045

4. Timing and energy consumption

The readout mechanism for this sensor consists of detecting all falling or rising edges

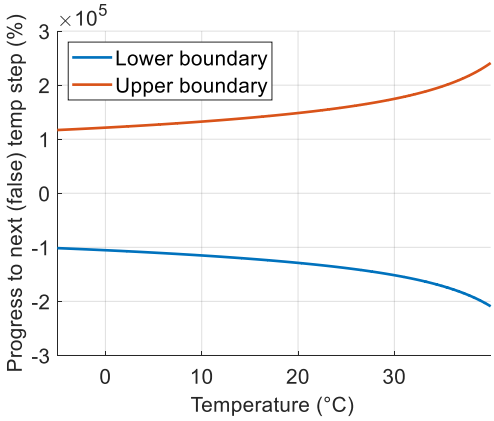

Fig. 8: Deviation from correct sensor reading concerning the distance of the next temperature value in percentage. Note that the values are times 10^5. This considerable deviation requires sensor calibration before use.

within a fixed observation window. In this setup, the selected switch creates parasitic capacitances that measure 13 pF between the pins and GND, affecting the integrator's charging times. Consequently, I_{R1} (Eq. (8)) is divided between the parasitic capacitance of the switch and the capacitor of the integrator, rated at 10 pF. As can be seen in Fig. 3, an increase in capacitance leads to a reduction in resolution. To keep the resolution constant, the observation time must be increased, as shown in Eq. (13) and Eq. (14), where the capacitance and the observation window have an inverse effect on the resolution n_{cycles}. The introduction of a capacitance of 2.2 nF counteracts the parasitic effect, but requires an

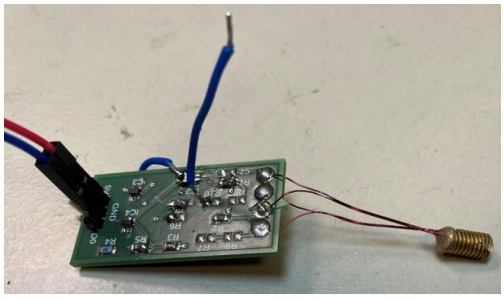

Fig. 9: Prototype implementing the core circuit. The measuring tip of the sensor is coated with a PU resin layer and encased in a brass sleeve to protect it from environmental influences.

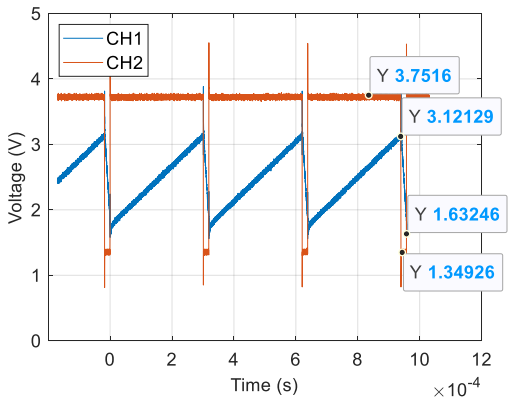

Fig. 10: Measurement of the core circuit. CH1 shows the voltage output of the integrator while CH2 displays the digital output of the Schmitt trigger.

extension of the observation time to 220 s. Using the approach described in [2], considering the charge flow on the integrator and reducing the observation time by the ratio of the charging and discharging times, the resistance value of the thermistors can be determined using

$$R_T = \sqrt{R_1 R_2 \left(\frac{t_{chg}}{t_{dchg}} - 1 \right)} \qquad (16)$$

The simulation of the circuit and the evaluation of this approach shows that an observation window of 10 s in conjunction with a sampling frequency of 1 MHz achieves the desired accuracy of 1 mK. The components required for the core circuit and an Adafruit Feathers MCU amount to 26.05 € for one sensor, not including the circuit board. The estimated power consumption for one measurement is 84.64 mWs.

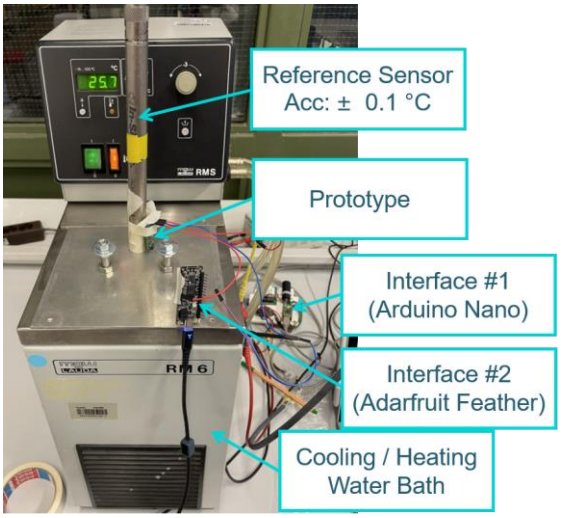

Fig. 11: Test setup. The sensor and the reference sensor of the Aqua TROLL 100 data logger are placed in a Lauda RM6 cooling water bath with the probes as close together as possible. The Arduino Nano reads the data logger, while the Adafruit Feather is connected to our board and adds the microcontroller for counting and data forwarding.

5. Implementation and testing

A first prototype, containing only the core circuit (Fig. 1), was built and tested (Fig. 9). An initial functional test of the integrator and the Schmitt trigger shows promising results (Fig. 10). The computing power is provided by an Adafruit Feather M4 Express, which performs floating point operations and establishes a connection to a computer for data exchange via a UART. The Adafruit Feather is connected to the digital pin of the core circuit and to GND and accesses the digital output of the circuit. A Lauda RM6 cooling water bath provides a thermally controlled environment. It contains five liters of liquid and regulates the temperature from -15 °C to +100 °C. A lid with two openings for the sensors closes the water bath. The reference sensor is an Aqua TROLL 100 data logger, accessed by an Arduino Nano via the SDI-12 interface reading temperature data from the reference sensor (Fig. 11). The Adafruit Feather tracks the duration of a low signal on the D0 pin of our temperature sensor within 10 seconds and calculates the ratio of the charging and the discharging time. It forwards this information to a laptop and calculates the temperature asynchronously during this experimental setup.

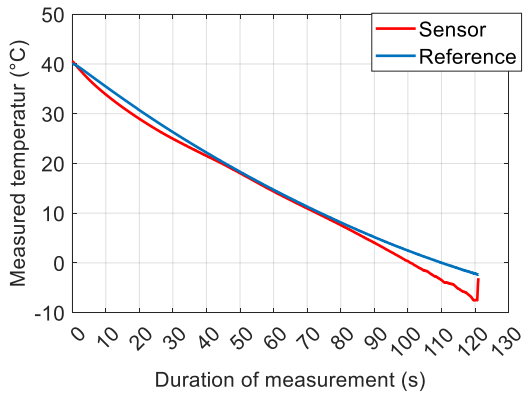

Fig. 12: Sensor and reference recording over the entire measuring range to obtain sensor calibration point data.

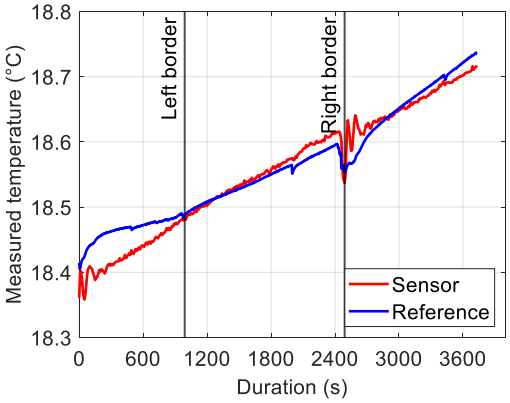

Fig. 13: Stability test with the temperature bath at room temperature. The area inside the margins is broken down in more detail in Fig. 14.

Tab. 4: Ratios of charge and discharge times from three different temperatures derive the thermistor resistances to be used for calibration.

Θ	t_{chg}/t_{dchg} mean of five	R_T
0 °C	*241.249*	*340999.214 Ω*
25 °C	*15.948*	*85057.244 Ω*
40 °C	*4.088*	*38658.782 Ω*

Tab. 5: Coefficients for the Steinhardt-Hart equation.

Coefficient	Value
A	1.62865e −3
B	1.2094e −4
C	2.2979e −7

The Arduino framework provides the core functions for programming the MCU. Sampling at 1 MHz requires a separate implementation, as the *micros()* frame function and the *digitalRead()* function do not allow repetitions within 1 µs. Instead, the program accesses the MCU's read registers directly.

5.1 Calibration

The calculation of the resistances of the thermistors from the ratio of charge and discharge times according to equation Eq. (16) serves as preparation for determining the coefficients of the Steinhardt-Hart equation for calculating the temperature from the sensor values (Eq. (1)). Measuring these ratios five times at a temperature of 0 °C, 25 °C, and 40 °C using the reference sensor Aqua TROLL 100 data logger leads to the derived thermistor resistance values in Tab. 4.

Using MATLAB, the previously calculated resistance values, and the three values of R_T *in Eq. (1), the coefficients are calculated according to*

Tab. 5.

5.2 Testing

Cooling the water bath to 0 °C after heating it up to 40 °C while measuring continuously with both sensors provides data for analyzing the performance of the sensor, as shown in Fig. 12. The minimum temperature is around 0 °C, as the water turns to ice in the current setup. The effects of calibration at the edges of the temperature range and at 25 °C are visible and show poor performance at lower temperatures. A second test is performed with the water bath at room temperature for one hour to determine the measurement resolution. The reference sensor exhibits non-linearity and takes approximately 15 minutes to return to a more reliable reading. An event occurred at around 12:30 (Fig. 13). The highlighted area is taken into account when checking the resolution of the sensor, which is below 10 mK (Fig. 14). By cooling down three times from 40 °C to 0 °C and heating up again to 40 °C, the reaction of the sensor to temperature changes and hysteresis is recorded within 450 minutes (Fig. 15). The sensor behavior shown in Fig. 12 can be seen within the hysteresis form. This is a combination of the calibration process and the thermal latency due to the large thermal mass of the brass body at the sensor tip.

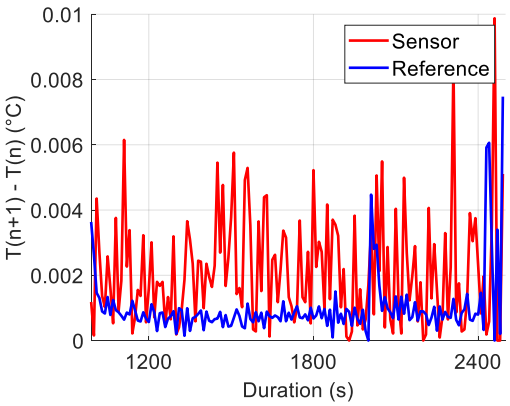

Fig. 14: Stability test at room temperature (18.5 °C). The stability is below 10 mK for most of the range shown.

6. Results and outlook

A sensor was designed based on an improved design by Skinner and Lambert. The design is promising, but a comprehensive investigation of the first proposed method for reading the sensor and improved approaches to sensor calibration need to be conducted next. A comprehensive investigation could also include the electrical characteristics of devices not considered, such as the operational amplifiers and the microcontroller, with the prospect of creating a digital twin of this sensor. The output of the Schmitt trigger should also be investigated, as a rail-to-rail output was expected. The results of the first measurements are promising, as the current calculations still offer a lot of room for improvement in calibration and temperature error correction, as can be seen in Fig. 8. Despite the difficult conditions for performing the test in terms of the desired temperature resolution, a sensor resolution of 6 mK and below was observed (Fig. 14). This is not yet within the desired range of 5 mK. The hysteresis shows the influence of the thermal mass and thus the thermal inertia, increased by the brass sleeve. It also shows the previously observed sensor behavior based on the calibration procedure, which has a better fit for a range of 10 °C to 20 °C. An improved version of this sensor will be developed based on the knowledge gained during development and testing.

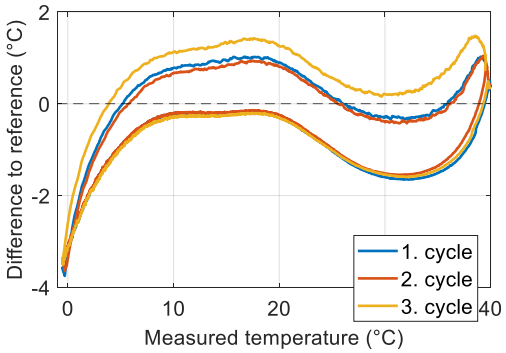

Fig. 15: Deviation of the sensor readings of the reference sensor and our prototype (sensor – reference). The upper curves show the cooling cycle, while the lower parts show the behavior during heating. A significant drift can be seen during the cooling of the third cycle.

References

[1] Z. Su et al., High-frequency submesoscale motions enhance the upward vertical heat transport in the global ocean, Journal of Geophysical Research: Oceans 125, 1-13 (2020); doi: 10.1029/2020JC016544

[2] J. Skinner and M. F. Lambert, Using smart sensor strings for continuous monitoring of temperature stratification in large water bodies, IEEE Sensors Journal 6(6), 1473-1481 (2006); doi: 10.1109/JSEN.2006.881373

[3] Van Haren, Philosophy and application of high-resolution temperature sensors for stratified waters. Sensors 18, 3184 (2018); doi: 10.3390/s18103184

[4] Pan, S., Makinwa, K.A.A. (2022).Wien bridge-based temperature sensors. In: Resistor-based Temperature Sensors in CMOS Technology. Analog Circuits and Signal Processing. Springer, Cham; doi: 10.1007/978-3-030-95284-6

[5] S. Steinhart and S. R. Hart, "Calibration curves for thermistors," Deep Sea Res., vol. 15, p. 497, 1968; doi: 10.1016/0011-7471(68)90057-0